Differentiation of Soil Conditions over Low Relief Areas Using Feedback Dynamic Patterns

A-Xing Zhu
State Key Lab. of Resources and Environmental Information Systems
Institute of Geographical Sciences and Natural Resources Research
Chinese Academy of Sciences
Beijing 100101, China

and
Dep. of Geography
Univ. of Wisconsin
Madison, WI 53706

Feng Liu*
State Key Lab. of Resources and Environmental Information Systems
Institute of Geographical Sciences and Natural Resources Research
Chinese Academy of Sciences
Beijing 100101, China

and
Graduate Univ.
Chinese Academy of Sciences
Beijing 100049, China

Baolin Li
Tao Pei
Chengzhi Qin
Gaohuan Liu
Yingjie Wang
State Key Lab. of Resources and Environmental Information Systems
Institute of Geographical Sciences and Natural Resources Research
Chinese Academy of Sciences
Beijing 100101, China

Yaning Chen
Key Lab. of Oasis Ecology and Desert Environment
Xinjiang Inst. of Ecology and Geography
Chinese Academy of Sciences
Urumqi, Xinjiang 830011, China

Xingwang Ma
Institute of Soil and Fertilizer
Xinjiang Academy of Agric. Sciences
Urumqi, Xinjiang 830000, China

Feng Qi
Dep. of Geology and Meteorology
Kean Univ.
Union, NJ 07083

Chenghu Zhou
State Key Lab. of Resources and Environmental Information System
Institute of Geographical Sciences and Natural Resources Research
Chinese Academy of Sciences
Beijing 100101, China

In many areas, such as plains and gently undulating terrain, easy-to-measure soil-forming factors such as landform and vegetation do not co-vary with soil conditions across space to the level that they can be effectively used in digital soil mapping. A challenging problem is how to develop a new environmental variable that co-varies with soil spatial variation under these situations. This study examined the idea that change patterns (dynamic feedback patterns) of the land surface, such as those captured daily by remote sensing images during a short period (6–7 d) after a major rain event, can be used to differentiate soil types. To examine this idea, we selected two study areas with different climates: one in northeastern China and the other in northwestern China. Images from the Moderate Resolution Imaging Spectroradiometer (MODIS) were used to capture land surface feedback. To measure feedback dynamics, we used spectral information divergence (SID). Results of an independent-samples t-test showed that there was a significant difference in SID values between pixel pairs of the same soil subgroup and those of different subgroups. This indicated that areas with different soil types (subgroup level) exhibited significantly different dynamic feedback patterns, and areas within the same soil type have similar dynamic feedback patterns. It was also found that the more similar the soil types, the more similar the feedback patterns. These findings could lead to the development of a new environmental covariate that could be used to improve the accuracy of soil mapping in low-relief areas.

Abbreviations: MODIS, Moderate Resolution Imaging Spectroradiometer; NDVI, normalized difference vegetation index; SID, spectral information divergence.

The soil–landscape relationship theory relates difficult-to-measure soil information, which includes soil type and soil properties, with some easy-to-obtain soil-forming environmental factors. This makes it possible to infer soil spatial variations from the easy-to-obtain environmental factors. In many areas, however, especially plains and gently undulating terrain, easy-to-observe factors such as landform characteristics and vegetation conditions cannot effectively reflect spatial variations of the soils (Logan, 1916; Ding et al., 1989; McKenzie and Austin, 1993; Levine et al., 1994; Mendonca Santos et al., 1997, 2000; McKenzie and Ryan, 1999; Odeh and McBratney, 2000; Iqbal et al., 2005).

Some researchers have attempted to address this issue using remote sensing techniques, mainly including three types of methods. The first type uses visual image interpretation to retrieve soil spatial variation. Ding et al. (1989) used Landsat Multispectral Scanner images to create a 1:500,000 soil map for cultivated plain areas in Jiangsu Province, China. Ziadat et al. (2003) tried to discriminate soil mapping units based on Landsat Thematic Mapper images across an area with level topography in the northern part of Jordan. Both efforts failed to produce good results, however, partially because of difficulties in visually interpreting soil-forming factors such as landform, lithology, vegetation, and hydrology.

The second type of method identifies soil differences through image classification techniques using multiband and multidate remotely sensed data. Based on this approach, Dobos et al. (2000) attempted to map the spatial variation of soils

Soil Sci. Soc. Am. J. 74:861–869
Published online 1 Feb. 2010
doi:10.2136/sssaj2008.0411
Received date 14 Dec. 2008.
*Corresponding author (liuf@lreis.ac.cn).

in a floodplain area of northern Hungary. Five basic Advanced Very High Resolution Radiometer (AVHRR) channels and the normalized difference vegetation index (NDVI) of five non-consecutive dates were selected to represent different stages of vegetative growth. Unfortunately, the approach was not effective because the selected imagery failed to capture information for distinguishing soil conditions. Kienast-Brown and Boettinger (2007) obtained land cover classes from supervised classification of Landsat Enhanced Thematic Mapper Plus images and then used these classes to discern the spatial variation of special soils (wet and saline soils) in a low-relief area in northern Utah. Wet and saline soils are special in that they have unique spectral signatures and show up as different land cover classes. Mapping other soil types over flat areas is still a challenge.

The third type of method incorporates remotely sensed images into spatial prediction models such as regression kriging for characterizing soil variation. Odeh and McBratney (2000) effectively predicted most of the soil spatial variation in the lower Namoi Valley of northwestern New South Wales in Australia using AVHRR images acquired in the absence of vegetation. Carré and Girard (2002) used both Système Pour l'Observation de la Terre (SPOT) images (three spectral bands and their derivative indices) and some terrain variables to map soil types in a nearly flat area situated in the south of the La Rochelle area on the French Atlantic seaboard. With this approach, however, a great deal of field sampling is required to quantitatively define the required spatial autocorrelation. This requirement makes this approach unsuitable for large areas.

In addition to the remote sensing methods described above, Bragato (2004) explored the combination of detailed field soil sampling and spatial interpolation (linear regression and geostatistics) to obtain the soil spatial distribution across flat floodplains. Again, the collection of a large number of field samples is time consuming and expensive. The nonlinearity of soil-forming processes and heterogeneity of soil conditions may also make these statistical and geostatistical methods unsuitable for soil mapping across large areas.

We have developed an approach that derives a new environmental variable that co-varies with soil spatial information across low-relief areas. The new variable is land surface feedback dynamics observed through multi-temporal satellite remote sensing data over a short period after a major rainstorm event.

MATERIALS AND METHODS

Method Overview

Suppose that there is a spatially uniform input to land surface; locations with different soil conditions would have different feedback to this input when other environmental conditions are the same. Thus, soil differences would be indicated by the differences in the land surface feedback patterns. Based on this idea, we used rainfall as the input to the land surface and assumed that the occurrence of the input event across a certain spatial extent is spatially uniform. Once the rainfall stops, the land surface starts to dry up. This drying process is the feedback of the land surface in response to the rainfall. The characteristics of this drying process at a given location during the next few days right after the rain event is referred to as the *land surface feedback dynamic pattern* for that location, which can be captured by remote sensors as changes in electromagnetic reflectance with time. The land surface feedback dynamic pattern is dependent on the surface conditions (such as vegetation and topography) as well as the soil conditions, assuming uniform rainfall across the area in question. If the surface conditions are the same or very similar, then the feedback pattern should be largely dependent on only the soil conditions. Differences in the feedback dynamic patterns between two locations can then be related to differences in the soils between these locations. Therefore, the spatial difference in the land surface feedback dynamic patterns has a potential to be used for identifying soil spatial variation.

Figure 1 illustrates three stages for implementing this idea. The first stage is to stimulate feedback. A major rainfall input is received by the land surface, and then during a short period after the rainfall event, the land surface produces dynamic feedback in response to this input. The second stage captures the stimulated feedback using the MODIS sensor and characterizes the feedback. The third stage relates differences in the feedback patterns to differences in soil types.

Study Areas

Two different study areas were used in this research: one in the Hailun area in northeast China, representing a semihumid environment (referred to as the Hailun study area), and the other in the Ili watershed in northwest China, representing an arid environment (referred to as the Ili study area). The two areas were chosen mainly because their landform and vegetation conditions cannot be effectively used to capture soil spatial variation.

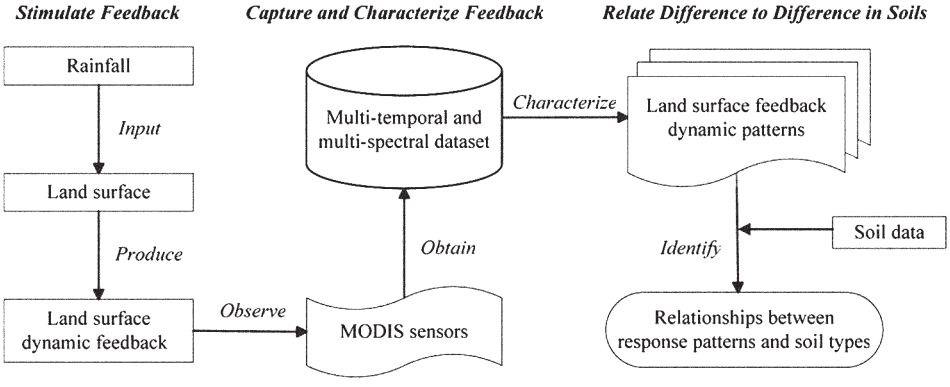

Fig. 1. Three stages for implementing the use of land surface feedback dynamic patterns to identify soil types.

The Hailun study area, approximately 1670 km^2, is located in the central part of Heilongjiang Province, China (47.00–47.27° N and 126.50–127.25° E) (Fig. 2). It is a floodplain area with low relief. The climate is semihumid, cold, temperate continental with a monsoon influence from the southeast. The mean annual temperature is 1.6°C and the mean annual precipitation is about 550 mm.

The elevation is between 160 and 250 m. Across most of the area, the slope gradient is <2°. The primary soil parent material is a loess-like subclay. The major soil subgroups are Typical Black Soil, Typical Meadow Soil, and Calcareous Meadow Soil. (The Chinese Classification System currently contains five major soil categories: order, suborder, group, subgroup, family, and series [Chinese Soil Taxonomy Research Group, 2001]. Categories at the subgroup level have been established for the entire nation. Categories at the family and series levels only exist at research sites, and are not available for broad coverage.) They exhibit great spatial variation. The area is cultivated with crops such as wheat (*Triticum aestivum* L.), soybean [*Glycine max* (L.) Merr.], and maize (*Zea mays* L.).

The Ili study area is situated in the Ili River watershed, which is surrounded by the Tianshan Mountains on three sides. It is about 35 km (north–south) by 82 km (east–west), and 470 km west of Ürümqi (43.78° N, 87.62° E), Xinjiang Uygur Autonomous Region, China (Fig. 3). The climate is arid, with a mean annual precipitation of 264 mm, a mean annual evaporation of 1630 mm, and a mean annual air temperature of 9.2°C. This study area is a portion of a pluvial-alluvial plain in the watershed and consists of several large, low-lying pluvial fans. Elevation in the area ranges from 533 to 970 m. Slope gradient is often <2°, with a mean <1°. The parent materials for soil development are characterized by Quaternary loess deposits. The area contains 14 distinct soil subgroups, including Irrigated Desert Soils, Meadow Solonchaks, Fluvo-Aquic soils, Light Sierozems, Typical Sierozems, Peat Bog Soils, Salinized Fluvo-Aquic Soils, Salinized Sierozems, Salinized Meadow Soils, Calcareous Meadow Soils, Meadow Bog Soils, Meadow Sierozems, Meadow Solonchaks, and Desert Aeolian soils. The main crops grown in this area include wheat, maize, cotton (*Gossypium hirsutum* L.) and oilseed rape (*Brassica napus* L. var. *napus*).

Stimulating Feedback

To stimulate effectively feedback, the following three requirements need to be met. The first is that the area of interest needs to experience a long period (>1 mo) of no to little rain so that the area is very dry and moisture becomes a limiting factor. The second is that the magnitude of the rainfall input should be large enough to force the land surface to produce a clear response. The third is that there can be no precipitation over the area in the 7 d or so immediately after the rainfall event (referred to as the *observation period*). The required rainfall events and observation periods were determined for each of the areas based on daily meteorological observations in the respective areas.

For the Hailun area, there was a heavy rainfall (18.9 mm) on 23 Apr. 2001 (Fig. 4). Before that, the area had experienced a long and dry winter. Furthermore, the early spring was characterized by little precipitation, dramatically increasing air temperature and evaporation. As a result, the land surface in the area was in a very dry state before the rainfall event. After the rainstorm event, no rainfall occurred in the region for >1 wk. In addition, soils across much of the area were exposed due to the fact that the natural vegetation coverage in this area was very limited and crops had not yet emerged. Therefore, the period from 24 April to 1 May was selected as the observation period.

Similarly, a major rainfall (11.5 mm) on 15 May 2001 was selected for the Ili area. At that time, crops in the area had just emerged and were still small and sparsely distributed. Hence, for this area, the period from 16 to 31 May was chosen as the observation period.

Capturing and Characterizing Feedback

Capturing Feedback

Due to high temporal resolution (1 d or less), MODIS sensors on board the polar orbiting satellites Terra and Aqua of the National Aeronautics and Space Administration provide a good platform for

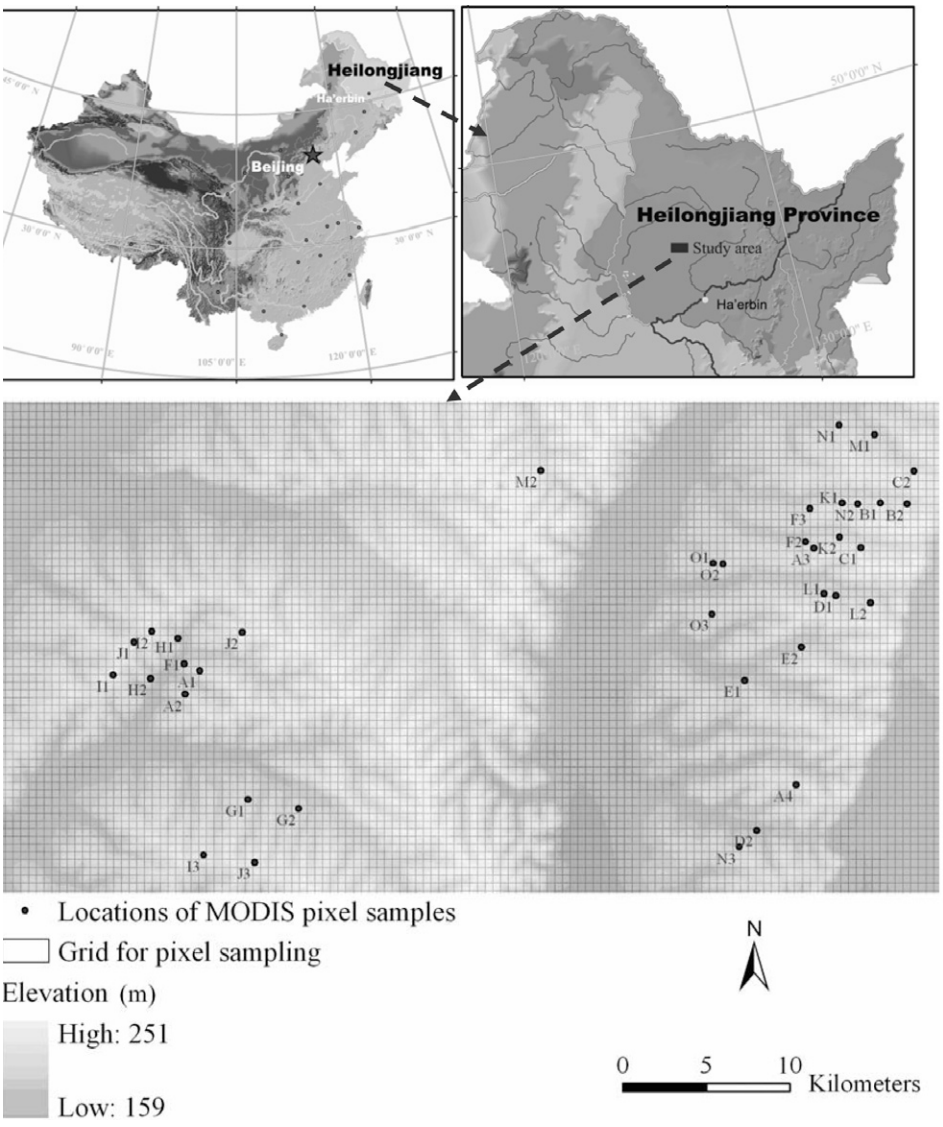

Fig. 2. Location of the Hailun study area and selected MODIS pixels with a relief map background.

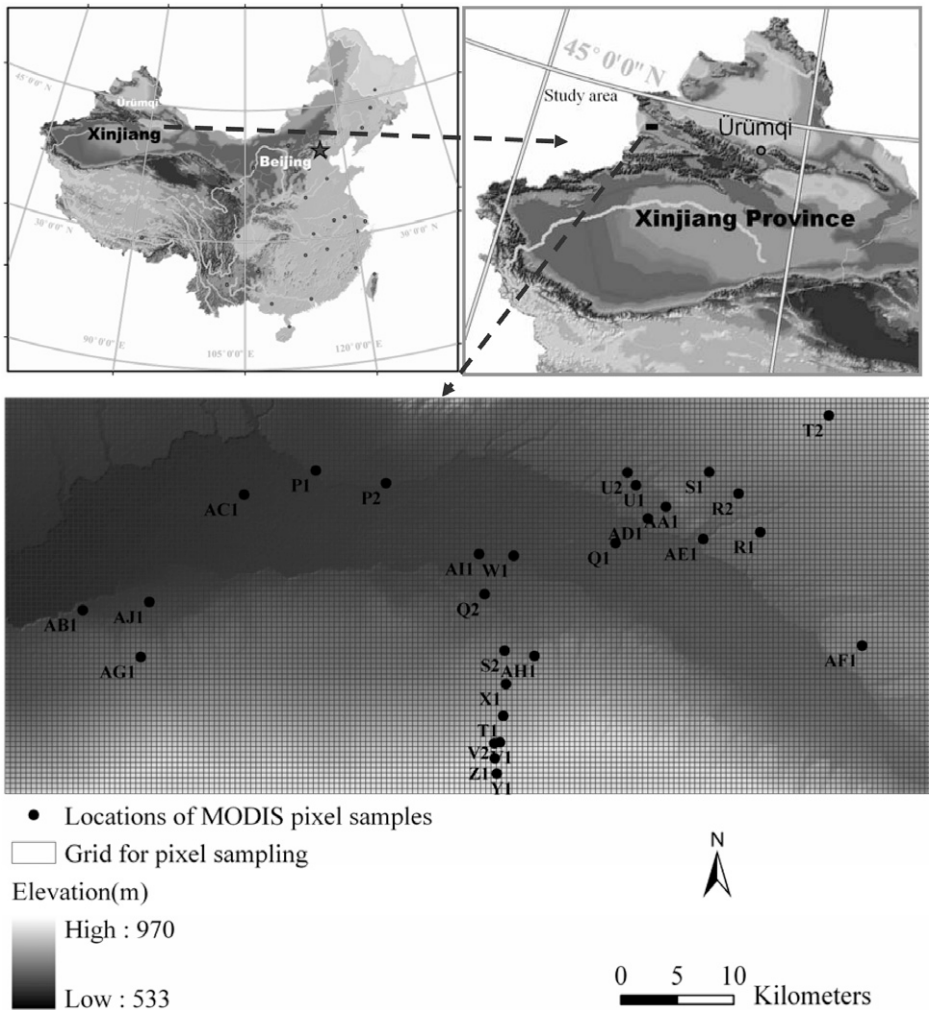

Fig. 3. Location of the Ili study area and selected MODIS pixels with a relief map background.

capturing the land surface dynamic feedback. Their moderate spatial resolution (250 m for Bands 1–2, 500 m for Bands 3–7, and 1000 m for Bands 8–36) and high geo-location precision are also suitable for land surface observations (Justice, 1998; Barnes et al., 1998, 2002; Salomonson et al., 2002; Wolfe et al., 1998, 2002). The following seven observation windows, mainly designed for land surface observation and research (Vermote and Vermeulen, 1999, p. 11–50), were selected for capturing feedback patterns: blue (459–479 nm), green (545–565 nm), red (620–670 nm), near infrared (NIR1: 841–876 nm, NIR2: 1230–1250 nm), and shortwave infrared (SWIR1: 1628–1652 nm; SWIR2: 2105–2155 nm). The MODIS daily surface reflectance (MOD09GHK, v004) at 500-m spatial resolution was used in this study. The data sets were obtained though the NASA Warehouse Inventory Search Tool (WIST, https://wist.echo.nasa.gov/api/).

The MODIS data are delivered in tiles, each covering an area of 10° latitude by 10° longitude. The Hailun area is covered by the tile H26V04. We acquired daily Terra MODIS land surface reflectance data within the selected observation period for this area. Due to the influence of cloud coverage, images acquired on 24 April, 30 April, and 1 May were of poor quality and not used. The daily Terra MODIS surface reflectance data for the period from 25 to 29 April (Day of the Year 115–119) in 2001 were ultimately used in our study. Similarly, the Ili area falls into tile H23V04 and thus images of this tile were obtained for the following dates: 16, 17, 18, 22, 23, 25, 27, and 31 May, for which good quality images were available.

Characterizing Differences in Feedback Dynamic Patterns

The captured feedback for each pixel contain spectral responses from multiple bands (n) over multiple dates (m). They were represented as a line, referred to as the *spectral-temporal response line* (Fig. 5). With the line format, the feedback were organized by date, and for each date the response (reflectance) was ordered by wavelength. Mathematically, the spectral-temporal response line can be expressed as

$$\mathrm{SR}_{x,y} = f_{x,y}(t,\lambda) \qquad [1]$$

where SR denotes the spectral response, which can be the digital number, surface reflectance, or surface radiance—we used surface reflectance in this study; t is time, corresponding to a series of dates during the observation period; λ is the wavelength of the electromagnetic wave, corresponding to a series of bands (seven in this study); and x and y are the coordinates in geographic space.

We used SID in this study to quantify the difference between the spectral-temporal response lines of any two MODIS pixels. Spectral

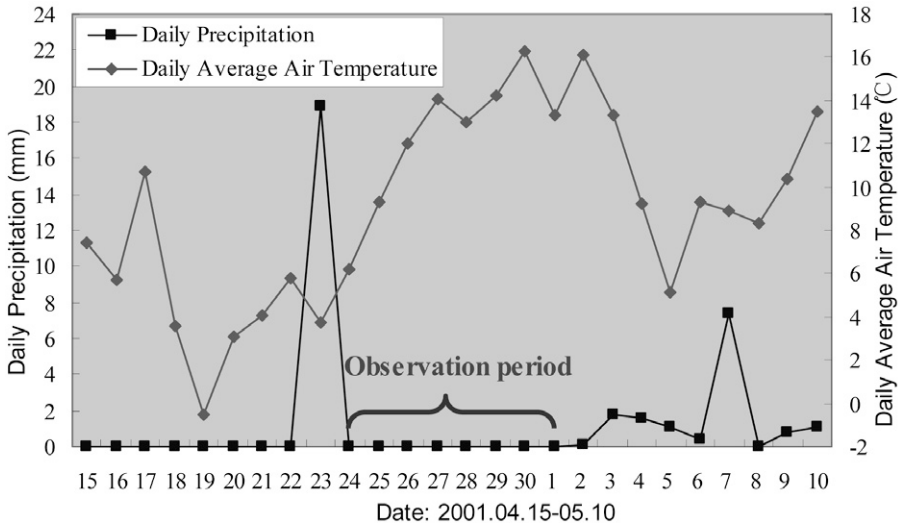

Fig. 4. Selection of observation period for the Hailun study area: 24 Apr. to 1 May 2001.

information divergence has been designed for quantitative analysis of spectral patterns organized in the line format. It can be defined in following way. Each pixel is considered to be a random variable, and its spectral histogram can be treated as its probability distribution. The discrepancy of probabilistic behaviors between the spectra of two pixels is the SID, which is used for characterizing spectral similarity and discrimination ability (Chang, 2000, 2003;Qin, 2009). We calculated the SID values of any two MODIS pixels within each study area using the following equations (Chang, 1999; van der Meer, 2006):

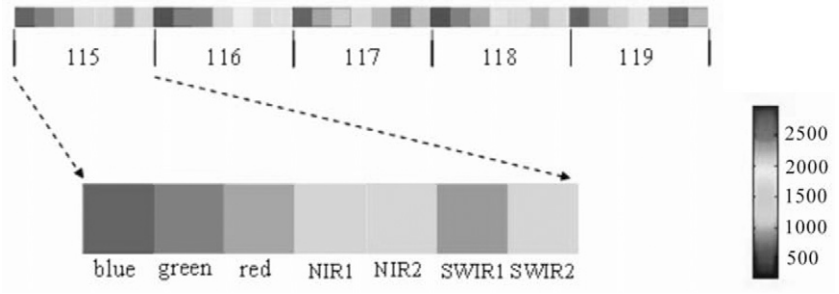

Fig. 5. Spectral-temporal response line. The captured feedback at a pixel are listed by date (Day of the Year 115–119) and for each date the responses (reflectance values) are organized by wavelength (NIR, near infrared; SWIR, shortwave infrared). For convenience, the surface reflectance is scaled by a factor of 10000.

$$\mathrm{SID}(X,Y)=D(X||Y)+D(Y||X) \quad [2]$$

$$D(X||Y)=\sum_{i=1}^{n}\sum_{j=1}^{m}p_{ij}\log\left(\frac{p_{ij}}{q_{ij}}\right) \quad [3]$$

$$D(Y||X)=\sum_{i=1}^{n}\sum_{j=1}^{m}q_{ij}\log\left(\frac{q_{ij}}{p_{ij}}\right) \quad [4]$$

$$p_{ij}=\frac{x_{ij}}{\sum_{i=1}^{n}\sum_{j=1}^{m}x_{ij}} \quad [5]$$

$$q_{ij}=\frac{y_{ij}}{\sum_{i=1}^{n}\sum_{j=1}^{m}y_{ij}} \quad [6]$$

where X and Y represent the feedback pattern at Pixels X and Y, respectively; $D(X||Y)$ is the relative entropy of Y with respect to X, which is also known as the Kullack–Leibler information function, directed divergence, or cross entropy (indicated with the || symbol); similarly, $D(Y||X)$ is the relative entropy of X with respect to Y; x_{ij} and y_{ij} are response elements for the ith band on the jth date for Pixels X and Y, respectively. Natural logarithms were used here; the measurement unit of SID is the *nat*. (A nat is a logarithmic unit of information or entropy, based on natural logarithms and powers of e; it is the fundamental unit of information using base e, while bit is the fundamental unit using base 2.) The values of SID range from zero to ∞. The more similar the spectral-temporal response lines between two MODIS pixels, the closer the SID is to zero. When the response lines are exactly the same, the SID is equal to zero.

Relating Differences in Feedback to Differences in Soils

The objective of this study was to examine whether a difference in land surface dynamic feedback patterns can be related to a difference in soils between the pixels. Thus, in this study we did not cover the entire study areas but focused on dozens of individual MODIS pixels in each of the two areas.

We selected the MODIS pixels where the land cover was homogeneous within each pixel and its surrounding area. In the Hailun area, we collected 37 MODIS pixels with bare soil. These pixels involved four different soil subgroups (Fig. 2). The soil subgroup data of the selected pixels in this area were obtained from the Soil Database of China, provided by the Institute of Soil Science, Chinese Academy of Sciences. For the Ili area, 28 field soil sampling points were collected and the soil subgroups of the 28 points were identified by local soil experts based on data from laboratory analyses (Yu, 2008, p. 8–18). We selected MODIS pixels that contained the 28 field sampling points (Fig. 3).

These selected MODIS pixels still had clear differences in landforms or vegetation even though they were from low-relief areas. To minimize the difference in feedback patterns due to differences in landforms or vegetation, it was necessary to organize the MODIS pixels into different groups according to elevation, slope gradient, east–west (EW) aspect, north–south (NS) aspect, and NDVI. All MODIS pixels within the same group were assumed to have very similar landforms and vegetation, while MODIS pixels from different groups had different landforms and vegetation.

For the Hailun area, with no significant vegetation cover during the selected observation period, the 37 MODIS pixels were grouped into 15 different groups based on elevation, slope gradient, EW aspect, and NS aspect. The terrain attribute values were derived from a Shuttle Radar Topography Mission digital elevation model at 90-m resolution. We labeled the 15 groups with letters from A to O. Each MODIS pixel was then labeled by the group label plus a number (Fig. 2). For example, A1 refers to MODIS pixel no. 1 in Group A. Eight of the 37 MODIS pixels (G1, G2, I1, I2, I3, J1, J2, and J3) had to be excluded due to the influence of clouds. The remaining 29 pixels, involving 12 different groups (Table 1), were used in our analysis.

For the Ili study area, with very sparse crops during the selected period, the 28 MODIS pixels were grouped according to elevation, slope gradient, EW aspect, NS aspect, and NDVI. Some of groups had only one pixel in them. These groups were excluded from further analysis. The remaining seven groups were labeled with letters from P to V. Table 2 shows the average landform and vegetation attributes of the seven groups. The MODIS pixels within these groups were coded as P1, P2, Q1, Q2, R1, R2, S1, S2, T1, T2, U1, U2, V1, and V2 (Fig. 3).

Clearly, the landform and vegetation within each group are very similar and differences in land surface feedback dynamic patterns can be assumed to be largely due to the differences in soil conditions. Based on this assumption, we related the differences in feedback patterns to the differences in soils. Then, with the purpose of examining the ability of land surface dynamic feedback patterns to differentiate soil subgroups, we analyzed the relationships between the SID values of any two MODIS pixels and their differences in soil subgroups.

Table 1. Average landform attributes of each landform–vegetation group within the Hailun area.

Landform-vegetation group	Elevation	Slope gradient	East–west aspect†	North–south aspect†
	m	°		
A	213.6	0.840	−0.590	0.365
B	210.4	1.075	0.100	0.820
C	215.0	1.100	0.000	0.755
D	199.2	1.140	−0.330	0.690
E	190.8	1.340	0.220	0.790
F	202.5	1.545	−0.675	0.665
H	195.0	1.565	0.855	0.080
K	204.2	1.065	−0.100	0.705
L	212.3	1.300	−0.130	0.720
M	202.7	1.085	0.630	0.675
N	205.5	0.760	−0.595	0.715
O	201.0	0.000	−0.015	0.950

† East–west aspect = sin(aspect); north–south aspect = cos(aspect).

RESULTS AND DISCUSSION

Differences in Feedback Patterns between Areas of Different Soil Subgroups and Areas of the Same Subgroup

Tables 3 and 4 show SID values and soil subgroups of MODIS pixel pairs from different landform–vegetation groups for the Hailun area, while Tables 5 and 6 show the same kinds of information for the Ili area. Tables 3 and 5 contain the pairs of pixels belonging to a same soil subgroup. Tables 4 and 6 contain the pairs of pixels from different soil subgroups. The two kinds of pixel pairs were classified as *same soil subgroup* and *different soil subgroups*, as shown in Table 7. An independent-samples *t*-test (Pallant, 2007) was used to compare SID values in the two classes. The SID values were normalized for this test.

Due to differences in land surface conditions and rainfall events, the magnitudes of the SID values for the two study areas were not at the same level. To consider MODIS pixels from the two areas together, SID values in Tables 3 to 6 were normalized using the standard score method (Pallant, 2007). This method considers every SID value as a score. A standard score, also called a *Z* score, is a dimensionless quantity derived by subtracting the population mean from an individual raw score and then dividing the difference by the population standard deviation. The mean and standard deviation of the SID values of all selected MODIS pixel pairs in each area were assumed to be those of the population for the area. As a result, all the SID values were converted into standard scores (Table 7).

Table 2. Average landform and vegetation attributes of each landform–vegetation group within the Ili area.

Landform–vegetation group	Elevation	Slope gradient	East–west aspect	North–south aspect	NDVI†
	m	degree			
P	574.0	0.374	0.224	−0.020	0.299
Q	606.5	0.691	0.103	−0.041	0.398
R	675.0	0.419	−0.075	−0.888	0.348
S	679.0	0.685	−0.430	0.898	0.276
T	767.5	0.869	0.462	0.621	0.306
U	641.5	1.227	−0.184	−0.908	0.266
V	814.5	1.419	−0.105	0.967	0.230

† Normalized difference vegetation index.

Table 3. Spectral information divergence (SID) of MODIS pixel pairs with the same soil subgroups and under several landform–vegetation conditions in the Hailun area; the mean SID ± SD are 0.0009 ± 0.0005.

Landform–vegetation group	Soil subgroup	Pixel pair	SID
			nat
A	Calcareous Meadow Soil	A1–A2	0.0004
F	Typical Meadow Soil	F2–F3	0.0008
H	Calcareous Meadow Soil	H1–H2	0.0018
K	Typical Meadow Soil	K1–K2	0.0009
N	Typical Meadow Soil	N1–N2	0.0007
O	Typical Black Soil	O1–O2	0.0002
		O1–O3	0.0015
		O2–O3	0.0009

Based on the data in Table 7, an independent-samples *t*-test was conducted. Levene's test for equality of variances resulted in an *F* value of 20.410 and a *P* value of 0.000. At a significance level of 0.05, the variances of the standard scores for the two classes

Table 4. Spectral information divergence (SID) values of MODIS pixel pairs with different soil subgroups and under several landform–vegetation conditions in the Hailun area; the mean SID ± SD are 0.0082 ± 0.0049.

Landform–vegetation group	Soil subgroup	Pixel pair	SID
			nat
A	Calcareous Meadow Soil	A1	0.0015
	Typical Meadow Soil	A3	
	Calcareous Meadow Soil	A2	0.0014
	Typical Meadow Soil	A3	
	Calcareous Meadow Soil	A1	0.0084
	Typical Black Soil	A4	
	Calcareous Meadow Soil	A2	0.0074
	Typical Black Soil	A4	
	Typical Meadow Soil	A3	0.0090
	Typical Black Soil	A4	
B	Typical Meadow Soil	B1	0.0062
	Typical Black Soil	B2	
C	Typical Meadow Soil	C1	0.0159
	Typical Black Soil	C2	
D	Typical Meadow Soil	D1	0.0043
	Typical Black Soil	D2	
E	Typical Meadow Soil	E1	0.0113
	Typical Black Soil	E2	
F	Calcareous Meadow Soil	F1	0.0039
	Typical Meadow Soil	F2	
	Calcareous Meadow Soil	F1	0.0044
	Typical Meadow Soil	F3	
L	Typical Meadow Soil	L1	0.0063
	Typical Black Soil	L2	
M	Typical Meadow Soil	M1	0.0160
	Typical Black Soil	M2	
N	Typical Meadow Soil	N1	0.0117
	Typical Black Soil	N3	
	Typical Meadow Soil	N2	0.0147
	Typical Black Soil	N3	

Table 5. Spectral information divergence (SID) values of MODIS pixel pairs with the same soil subgroups and under several landform-vegetation conditions in the Ili area; the mean SID ± SD are 0.0016 ± 0.0020.

Landform–vegetation group	Soil subgroup	Pixel pair	SID
			nat
U	irrigated desert soil	U1–U2	0.0030
V	light Sierozem	V1–V2	0.0002

were assumed to be unequal because the P value was <<0.05. Consequently, an unequal-variance t-test was used. The results of the t-test showed that $t = -6.878$ and $P = 0.000$. The value of P is <<0.05. Due to this, it can be considered that there is significant difference in the standard scores between the same soil subgroup class (mean = −0.925 and SD = 0.106) and the different soil subgroups class (mean = 0.463 and SD = 0.890). This indicates that the SID values between the two classes are significantly different.

Specifically, for the Hailun area, the SID values of pixel pairs from the same soil subgroup class (Table 3) ranged from 0.0002 to 0.0018, with the mean and SD being 0.0009 and 0.0005, respectively. Pixel pairs from the different soil subgroups class (Table 4), however, showed higher SID values between 0.0014 and 0.0160, with a mean of 0.0082 and a SD of 0.0049. The pattern repeated itself for the Ili area. The SID values in Table 6 are much higher than those in Table 5. Therefore, pixels belonging to different soil subgroups show significantly larger SID values, while pixels within the same soil subgroup have obviously smaller SID values. This means that areas with different soil subgroups exhibit significantly different dynamic feedback patterns, while areas within the same soil subgroup have obviously similar dynamic feedback patterns.

Change in Differences of Feedback Patterns with Differences in Soil Types

In Fig. 6, 7, and 8, the vertical axis represents the SID between the land surface feedback dynamic patterns of MODIS pixel pairs, and the horizontal axis denotes MODIS pixel pairs that are ordered according to the degree of difference between soil subgroups. These figures indicate that SID values increase with the degree of difference in soil types.

Specifically, within Landform–Vegetation Group A (see Fig. 6), the MODIS pixel pair A1–A2 belongs to the same soil subgroup (Calcareous Meadow Soil); pairs A1–A3 and A2–A3 both are from different soil subgroups (Calcareous Meadow Soil and Typical Meadow Soil) but within the same soil group (Meadow Soil); and pairs A1–A4, A2–A4, and A3–A4 are from different soil groups (Meadow Soil and Black Soil). From the left of the horizontal axis to the right in Fig. 6, there is an obvious increase with difference between soil types. Correspondingly, for the pixel pair A1–A2, the SID is fairly low at only 0.0004. Moving from A1–A2 to the pairs A1–A3 and A2–A3, SID values rise markedly to 0.0015 and 0.0014. For pairs A1–A4, A2–A4, and A3–A4, SID values climb farther dramatically to 0.0084, 0.0074, and 0.0090, respectively. The same trend can be seen in Landform–Vegetation Groups F and N (see Fig. 7 and 8). In addition, it should be noted that the MODIS pixels from different landform–vegetation groups are not comparable because they have different landforms and vegetation. Therefore, there is remarkable consistency between the differences in land surface feedback dynamic patterns and those of soil subgroups. The more similar the soil types are, the more similar their dynamic feedback patterns.

Table 6. Spectral information divergence (SID) values of MODIS pixel pairs with different soil subgroups and under several landform–vegetation conditions in the Ili area; the mean SID ± SD are 0.0462 ± 0.0269.

Landform–vegetation group	Soil subgroup	Pixel pair	SID
P	Irrigated Desert Soil	P1	0.0301
	Typical Sierozem	P2	
Q	Fluvo-Aquic Soil	Q1	0.0130
	Salinized Sierozems	Q2	
R	Calcareous Meadow Soil	R1	0.0416
	Fluvo-Aquic Soil	R2	
S	Fluvo-Aquic Soil	S1	0.0792
	Meadow Solonchak	S2	
T	Light Sierozem	T1	0.0670
	Typical Sierozem	T2	

Table 7. Standard scores derived from normalizing spectral information divergence (SID) values in Tables 3 to 6.

Class	Pixel pair	Standard SID score
Same soil subgroup	A1–A2	−0.9946
Same soil subgroup	F2–F3	−0.9186
Same soil subgroup	H1–H2	−0.7286
Same soil subgroup	K1–K2	−0.8996
Same soil subgroup	N1–N2	−0.9376
Same soil subgroup	O1–O2	−1.0326
Same soil subgroup	O1–O3	−0.7856
Same soil subgroup	O2–O3	−0.8996
Same soil subgroup	U1–U2	−0.9836
Same soil subgroup	V1–V2	−1.0741
Different soil subgroups	A1–A3	−0.7856
Different soil subgroups	A2–A3	−0.8046
Different soil subgroups	A1–A4	0.5254
Different soil subgroups	A2–A4	0.3354
Different soil subgroups	A3–A4	0.6394
Different soil subgroups	B1–B2	0.1074
Different soil subgroups	C1–C2	1.9505
Different soil subgroups	D1–D2	−0.2536
Different soil subgroups	E1–E2	1.0764
Different soil subgroups	F1–F2	−0.3296
Different soil subgroups	F1–F3	−0.2346
Different soil subgroups	L1–L2	0.1264
Different soil subgroups	M1–M2	1.9695
Different soil subgroups	N1–N3	1.1524
Different soil subgroups	N2–N3	1.7225
Different soil subgroups	P1–P2	−0.1080
Different soil subgroups	Q1–Q2	−0.6605
Different soil subgroups	R1–R2	0.2636
Different soil subgroups	S1–S2	1.4784
Different soil subgroups	T1–T2	1.0843

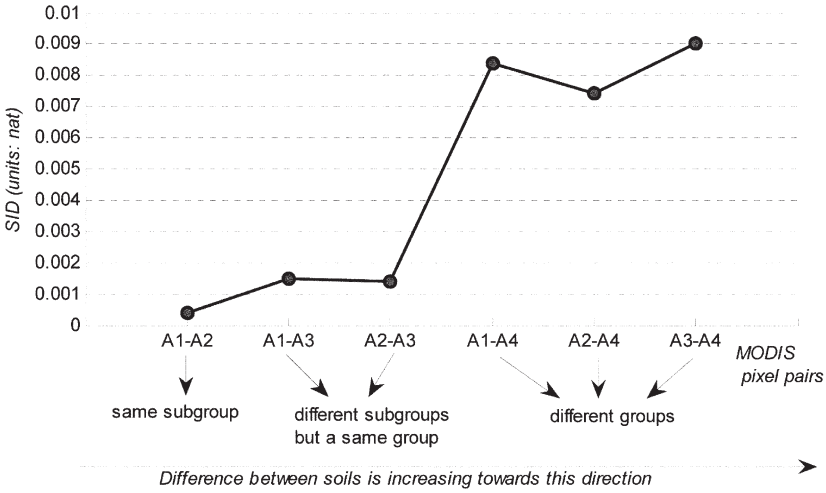

Fig. 6. Spectral information divergence (SID) values of MODIS pixel pairs within Landform–Vegetation Group A.

Based on the results and analyses above, it can be concluded that the differences observed between land surface feedback dynamics have the ability to capture effectively the differences in soil conditions between different pixels. The MODIS land surface observation data capable of providing this information are only available at spatial resolutions of 250 m (Bands 1–2) and 500 m (Bands 3–7), thereby making MODIS only suitable for digital soil mapping at coarse levels. The concept presented here, however, offers the potential for detailed mapping when remote sensing data become available at higher spatial and temporal resolutions.

CONCLUSIONS

We presented an idea of relating the difference in land surface feedback dynamic patterns after a major event to the difference in soil conditions at different locations. Land surface feedback dynamic patterns are defined as the pattern of change in reflectance captured by MODIS images during a short period at a daily interval after a major rain event. The difference in land surface feedback dynamic patterns between pixels was hypothesized to be highly related to the difference in soil conditions at these pixels, given that other surface conditions (mainly landform and vegetation) are the same.

Studies in the Hailun area of Heilongjiang Province and the Ili area of Xinjiang Province were conducted to evaluate this hypothesis and the associated methods. The results from the two areas indicated that areas with different soil subgroups exhibit significantly different dynamic feedback patterns and that areas belonging to the same soil subgroup have similar patterns. It was also found that the more similar the soil types, the more similar their response patterns. This leads to the conclusion that the land surface feedback dynamic patterns can be used to differentiate soil types effectively.

The findings reported here are encouraging and promising, and could lead to the development of a new environmental covariate that reflects soil spatial variations. In particular, this new covariate could be used to improve the accuracy of digital soil mapping over areas, such as flat terrain, where easy-to-measure soil-forming factors (such as topographic and vegetation information) are ineffective in revealing soil spatial variation.

This research provides another way to apply remote sensing data in environmental studies, such as natural resource mapping, habitat mapping, and delineation of areas sensitive to management plans. It must be noted, however, that future work is needed to examine these findings in the context of other landscape settings such as those with different vegetation cover densities and different climatic conditions. New metrics also need to be

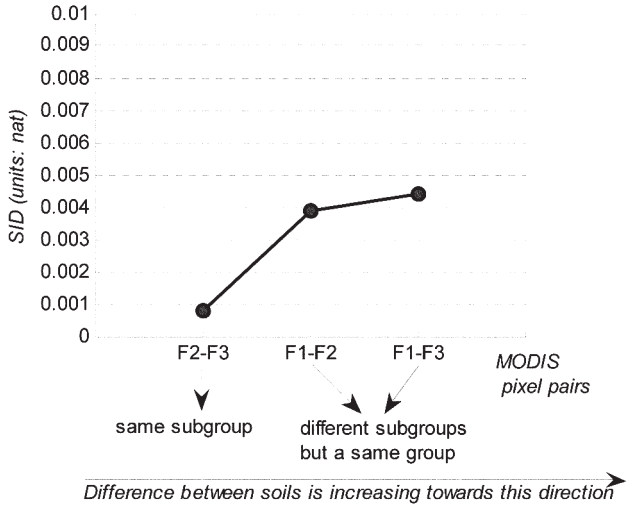

Fig. 7. Spectral information divergence (SID) values of MODIS pixel pairs within Landform–Vegetation Group F.

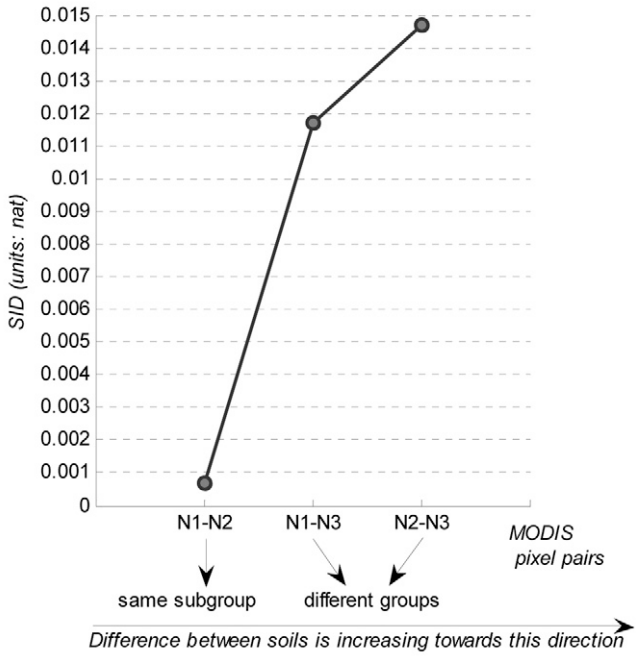

Fig. 8. Spectral information divergence (SID) values of MODIS pixel pairs within Landform–Vegetation Group N.

developed to assess the difference in land surface feedback dynamic patterns organized in the spectral-temporal surface format.

ACKNOWLEDGMENTS

This work was supported by the National Basic Research Program of China (2007CB407207), the National Key Technology R&D Program of China (2007BAC15B01), the National Natural Science Foundation (Project No.: 40971236), the support for Innovation from the State Key Laboratory of Resources and Environmental Information Systems, and the Vilas Trustees via the Vilas Associate Program at the University of Wisconsin-Madison. We thank all members of the Detailed Geographical Process Modeling group at the State Key Laboratory of Resources and Environmental Information Systems at the Institute of Geographic Sciences and Natural Resources Research of the Chinese Academy of Sciences for their encouragement and discussion on the work presented here.

REFERENCES

Barnes, W.L., T.S. Pagano, and V.V. Salomonson. 1998. Prelaunch characteristics of the Moderate Resolution Imaging Spectroradiometer (MODIS) on EOS-AM1. IEEE Trans. Geosci. Remote Sens. 36:1088–1100.

Barnes, W.L., X. Xiong, and V.V. Salomonson. 2002. Status of Terra MODIS and Aqua MODIS. p. 970–972. *In* IEEE IGARSS'02 Symp. Proc., Toronto, Canada. 24–28 June 2002. Vol. 2. IEEE Geosci. Remote Sens. Soc., Piscataway, NJ.

Bragato, G. 2004. Fuzzy continuous classification and spatial interpolation in conventional soil survey for soil mapping of the lower Piave plain. Geoderma 118:1–16.

Carré, F., and M.C. Girard. 2002. Quantitative mapping of soil types based on regression kriging of taxonomic distances with landform and land cover attributes. Geoderma 110:241–263.

Chang, C.I. 1999. Spectral information divergence for hyperspectral image analysis. p. 509–511. *In* IEEE IGARSS'99 Symp. Proc., Hamburg, Germany. Vol. 1. 28 June–2 July 1999. IEEE Geosci. Remote Sens. Soc., Piscataway, NJ.

Chang, C.I. 2000. An information theoretic-based approach to spectral variability, similarity and discrimination for hyper-spectral image analysis. IEEE Trans. Inf. Theory 46:1927–1932.

Chang, C.I. 2003. Hyperspectral imaging: Techniques for spectral detection and classification. Kluwer Acad. Publ., Dordrecht, the Netherlands.

Chinese Soil Taxonomy Research Group. 2001. Keys to Chinese Soil Taxonomy. 3rd ed. Univ. of Science and Technology of China Press, Hefei.

Ding, Y., S. Xu, and K. Zhu. 1989. Application of remote sensing techniques on 1:500,000 soil mapping in Nanjing, Jiangsu Province, China. (In Chinese.) Turang 6:304–306.

Dobos, E., E. Micheli, M.F. Baumgardner, L. Biehl, and T. Helt. 2000. Use of combined digital elevation model and satellite radiometric data for regional soil mapping. Geoderma 97:367–391.

Iqbal, J., J.A. Thomasson, J.N. Jenkins, P.R. Owens, and F.D. Whisler. 2005. Spatial variability analysis of soil physical properties of alluvial soils. Soil Sci. Soc. Am. J. 69:1338–1350.

Justice, C.O. 1998. The Moderate Resolution Imaging Spectroradiometer (MODIS): Land remote sensing for global change research. IEEE Trans. Geosci. Remote Sens. 36:1228–1249.

Kienast-Brown, S., and J.L. Boettinger. 2007. Land cover classification from Landsat imagery for mapping dynamic wet and saline soils. p. 235–244. *In* P. Lagacherie et al. (ed.) Digital soil mapping: An introductory perspective. Dev. Soil Sci. 31. Elsevier, Amsterdam.

Levine, L.R., R.G. Knox, and W.T. Lawrence. 1994. Relationships between soil properties and vegetation at the Northern Experimental Forest, Howland, Maine. Remote Sens. Environ. 47:231–241.

Logan, W.N. 1916. The soils of Mississippi. Tech. Bull. 7. Mississippi State Univ., Mississippi State.

Mendonca Santos, M.L., C. Guenat, M. Bouzelbuodjen, and F. Golay. 2000. Three-dimensional GIS cartography applied to the study of the spatial variation of soil horizons in a Swiss floodplain. Geoderma 97:351–366.

Mendonca Santos, M.L., C. Guenat, C. Thevoz, F. Bureau, and J.C. Vedy. 1997. Impacts of embanking on the soil–vegetation relationships in a floodplain ecosystem of a pre-alpine river. Global Ecol. Biogeogr. Lett. 6:339–348.

McKenzie, N.J., and M.P. Austin. 1993. A quantitative Australian approach to medium and small scale surveys based on soil stratigraphy and environmental correlation. Geoderma 57:329–355.

McKenzie, N.J., and P.J. Ryan. 1999. Spatial prediction of soil properties using environmental correlation. Geoderma 89:67–94.

Odeh, I.O.A., and A.B. McBratney. 2000. Using AVHRR images for spatial prediction of clay content in the Lower Namoi Valley of eastern Australia. Geoderma 97:237–254.

Pallant, J.F. 2007. SPSS survival manual. 3rd ed. Allen & Unwin, Sydney, NSW, Australia.

Qin, J., T.F. Burks, M.A. Ritenour, and W.G. Bonn. 2009. Detection of citrus canker using hyperspectral reflectance imaging with spectral information divergence. J. Food Eng. 93:183–191.

Salomonson, V.V., W.L. Barnes, X. Xiong, S. Kempler, and E. Masuoka. 2002. An overview of the Earth Observing System MODIS instrument and associated data systems performance. p. 1174–1176. *In* IEEE IGARSS'02 Symp. Proc., Toronto, Canada. 24–28 June 2002. Vol. 2. IEEE Geosci. Remote Sens. Soc., Piscataway, NJ.

van der Meer, F. 2006. The effectiveness of spectral similarity measures for the analysis of hyperspectral imagery. Int. J. Appl. Earth Observ. Geoinf. 8:3–17.

Vermote, E.F., and A. Vermeulen. 1999. MODIS: Algorithm technical background document. Atmospheric correction algorithm: Spectral reflectance (MOD09), version 4.0. NASA contract NAS5–96062. Goddard Space Flight Ctr., Greenbelt, MD.

Wolfe, R.E., M. Nishihama, A.J. Fleig, J.A. Kuyper, D.P. Roy, J.C. Storey, and F.S. Patt. 2002. Achieving sub-pixel geolocation accuracy in support of MODIS land science. Remote Sens. Environ. 83:31–49.

Wolfe, R.E., D.P. Roy, and E. Vermote. 1998. MODIS land data storage, gridding, and compositing methodology: Level 2 Grid. IEEE Trans. Geosci. Remote Sens. 36:1324–1338.

Yu, X.X. 2008. Soil quality assessment for newly cultivated lands in Eli basin, Xinjiang. B.A. thesis. Agric. Univ. of China, Beijing.

Ziadat, F.M., J.C. Taylor, and T.R. Brewer. 2003. Merging Landsat TM imagery with topographic data to aid soil mapping in the Badia region of Jordan. J. Arid Environ. 54:527–541.